



**The Abdus Salam  
International Centre for Theoretical Physics**



**2163-31**

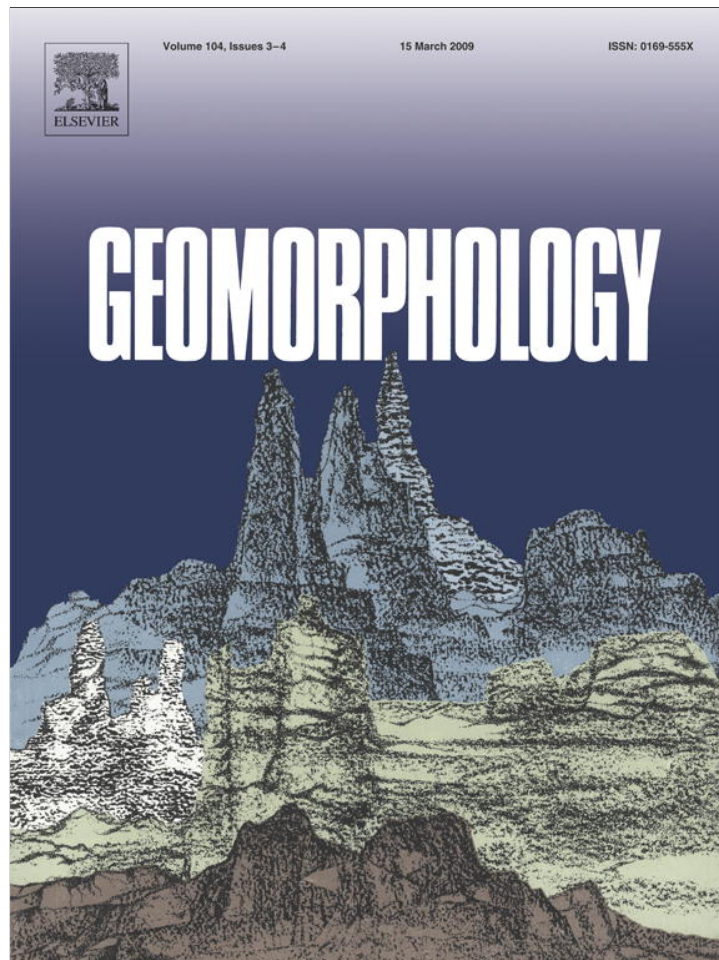
**College on Soil Physics: Soil Physical Properties and Processes under  
Climate Change**

*30 August - 10 September, 2010*

**Sand transport under increased lateral jetting of raindrops induced by wind**

Gunay Erpul  
*University of Ankara  
Turkey*

Provided for non-commercial research and education use.  
Not for reproduction, distribution or commercial use.



This article appeared in a journal published by Elsevier. The attached copy is furnished to the author for internal non-commercial research and education use, including for instruction at the authors institution and sharing with colleagues.

Other uses, including reproduction and distribution, or selling or licensing copies, or posting to personal, institutional or third party websites are prohibited.

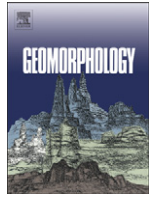
In most cases authors are permitted to post their version of the article (e.g. in Word or Tex form) to their personal website or institutional repository. Authors requiring further information regarding Elsevier's archiving and manuscript policies are encouraged to visit:

<http://www.elsevier.com/copyright>



Contents lists available at ScienceDirect

# Geomorphology

journal homepage: [www.elsevier.com/locate/geomorph](http://www.elsevier.com/locate/geomorph)

## Sand transport under increased lateral jetting of raindrops induced by wind

G. Erpul<sup>a,\*</sup>, D. Gabriels<sup>b</sup>, W.M. Cornelis<sup>b</sup>, H. Samray<sup>a</sup>, T. Guzelordu<sup>a</sup><sup>a</sup> Department of Soil Science, Faculty of Agriculture, University of Ankara, 06110 Diskapi-Ankara, Turkey<sup>b</sup> Department of Soil Management and Soil Care, Ghent University, Coupure Links 653, B 9000 Ghent, Belgium

### ARTICLE INFO

#### Article history:

Received 6 May 2008

Received in revised form 16 August 2008

Accepted 22 August 2008

Available online 5 September 2008

#### Keywords:

Sand transport

Rain incidence angle

Raindrop lateral jetting

Compressive stress

Shear stress

### ABSTRACT

Wind tunnel experiments for 'Raindrop Detachment and Wind-Driven Transport' (RD–WDT) process were conducted under improved lateral jetting induced by wind velocities of 6.4, 10, and 12 m s<sup>-1</sup> at nozzle operating pressures of 75, 100, and 150 kPa. Wind-driven rainfalls were also incident on the windward and leeward slopes of 4° and 9° to have a broad variation in the angle of incidence. The objective of this experimental set-up was to distinguish the roles of both impact components of obliquely striking wind-driven raindrops on RD and wind on WDT. Raindrop impact components and reference horizontal wind were quantified by normal ( $E_{tz}$ ) and horizontal ( $E_{tx}$ ) kinetic energy fluxes and wind shear velocity ( $u_*$ ), respectively, to physically model the process of RD–WDT. The results showed, at each level of  $u_*$ , differential sand transport rates by RD–WDT ( $q_{m(RD-WDT)}$ ) occurred depending on the magnitude of raindrop impact components, and  $q_{m(RD-WDT)}$  increased as the relative contribution of  $E_{tz}$  increased. Although  $E_{tx}$  was more correlated with  $q_{m(RD-WDT)}$  than  $E_{tz}$ , the extreme increases in  $E_{tx}$  at the expense of  $E_{tz}$  brought about no increases but decreases in  $q_{m(RD-WDT)}$ . An RD–WDT model was built under the process of examining the discrete effects of  $E_{tz}$  and  $E_{tx}$  on RD together with  $u_*$  and resulted in a better coefficient of determination ( $R^2=0.89$ ) than only total kinetic energy ( $E_t$ ) did alone with  $u_*$  ( $R^2=0.84$ ). In this study,  $E_{tx}$  was strongly related to  $u_*$  and not to  $E_{tz}$ , which was the principal difference from the previous rainsplash studies, which relied on the compensatory lateral jet development by the compressive pressure build-up at the raindrop–soil interface. Including  $E_{tx}$  in the RD–WDT model both separated the distinct role of each raindrop impact component in RD and improved the performance of  $u_*$  in WDT by better distinguishing its interaction with  $E_{tx}$ , which was not explicitly separated in previous models of RD–WDT.

© 2008 Elsevier B.V. All rights reserved.

### 1. Introduction

Kinnell (1999, 2005) reviewed the modes of raindrop impact-induced erosion processes and prediction. Of those, the mode of "Raindrop Detachment and Splash Transport" (RD–ST) takes place prior to the development of runoff, and clearly, in this case there is no transport of detached particles other than downslope gradient in the system. There are many studies of explaining the relationship between slope gradient and RD–ST (Savat and Poesen, 1981; Poesen and Savat, 1981; Moeyersons, 1983; Poesen, 1985; Riezebos and Epema, 1985; Wright, 1986, 1987), and recently, Furbish et al. (2007) gives the details of the transfer of momentum from raindrops to sand particles that contribute downslope transport of those for RD–ST. They described this momentum-transfer process under controlled laboratory conditions using high-speed images of drop impacts on sand targets. The conclusion they arrived at was that, as slope gradient increased, more sand particles moved downslope and move farther downslope than upslope. The greatest radial distance that a sand grain moved was around 20 cm or less in their study. Because of this, RD–ST

is generally described as a transport-limited process, particularly when it functions on large areas (Kinnell, 1999, 2005).

On the other hand, a transport process in which soil particles are detached by raindrop impact and afterward carried by wind instead of slope gradient is known as 'Splash-Saltation Transport' (SST) or described as 'Raindrop Detachment and Wind-Driven Transport' (RD–WDT) (De Ploey, 1980; Jungerius et al., 1981; Rutin, 1983; Jungerius and Dekker, 1990; De Lima et al., 1992; Erpul et al., 2002, 2004; Cornelis et al., 2004a,b). This system operates until runoff onset during wind-driven rains, but its transport (WDT) is independent of slope gradient and aspect (Erpul et al., 2004) as wind is the transporting agent. Unlike RD–ST, RD–WDT can significantly contribute to the total sediment transport from interrill areas (Erpul, 2001; Erpul et al., 2003a) and can transport particles as far as 7 m (Erpul et al., 2002, 2004) compared to the limited travel distance of RD–ST (Furbish et al., 2007). Depending on the prevailing wind direction, either uphill or downhill transport of sediments can occur by RD–WDT (Erpul et al., 2002; Visser and Sterk, 2007). Additionally, in contrast to the transport-limited system of RD–ST, RD–WDT could be a detachment-limited system because RD significantly varies with the variations in raindrop trajectory and frequency due to the changes in the angle of raindrop incidence (Erpul et al., 2003b).

\* Corresponding author. Tel.: +90 312 596 1796; fax: +90 312 317 8465.  
E-mail address: [erpul@agri.ankara.edu.tr](mailto:erpul@agri.ankara.edu.tr) (G. Erpul).

Clearly, RD–WDT could contribute to soil losses during storm events when intense rains and strong winds work together. Goossens et al. (2000) reported that spatial variations in rainfall during the rain events were the major cause of the differences in splash drift over the field and the wind caused oblique rainfall and an extra-displacement of the soil particles in the downwind direction. Erpul et al. (2003a), by wind tunnel studies under wind-driven simulated rains, comparing RD–WDT with the ‘Raindrop Detachment and Raindrop-Induced Flow Transport (RD–RIFT) (Kinnell, 1999, 2005), showed that soil loss by RD–WDT was a significant process that should be considered to assess interrill erosion, and the contribution of the process to the total sediment transport increased as the wind velocity to drive simulated rains increased from 6 m s<sup>-1</sup> to 14 m s<sup>-1</sup>. Warburton (2003) also indicated that wind erosion, in the form of RD–WDT, was a significant process in the UK uplands where winds were strong and persistent and the rainfall was high. Vieira et al. (2004) presented the influence of oblique rainfall on the genesis of the coarse sand accumulations and emphasized the importance of RD–WDT as the main transportation mechanism. Foulds and Warburton (2007a,b) reported that peat erosion caused by the integrated action of wind and rain might be a more important process than hitherto reported in UK upland areas. Their measurements confirmed that there was a previously unreported rapid switch in process regime between wind-driven rainfall and dry blow deflation in blanket peat environments.

The process of RD–WDT evidently requires the integrated action of both rain and wind (Choi, 1993; Blocken and Carmeliet, 2000, 2002, 2004; Blocken et al., 2005, 2006), and it is prompted by raindrop impacts instead of wind shear stress unless the effects on the velocity, frequency, and angle of impacting raindrops are considered. In other terms, the entrainment rate of particles depends on raindrop impacts and the energy state and the vector of which change with wind (Pedersen and Hasholt, 1995; Erpul, 2001; Erpul et al., 2003b). The wind comes into play not only in changing the raindrop impact parameters but also in transporting already raindrop-detached soil particles. In RD–WDT, it is now well known that RD is a key mechanism; and it is therefore desirable to develop a better approach to the RD–ST system which was developed for vertical windless rains, and can no longer be adequate to explain dislodgement rate for RD–WDT.

Kinnell (2005) gives a conceptual basis of RD–ST by the following equation for the cases in which slope gradient determines the transport efficiency and wind is not a driving factor:

$$q_{RD-ST} = k_{RD-ST} E_f [f(S)]. \quad (1)$$

Where  $q_{RD-ST}$  is the amount of material transported by RD–ST,  $k_{RD-ST}$  is the soil erodibility associated by RD–ST,  $E_f$  is the effective kinetic energy of impacting raindrops, and  $f(S)$  is a function that varies with slope gradient ( $S$ ). RD and ST can be described by linear or non-linear functions of rainfall parameters and slope gradient, respectively (Moeyersons and De Ploey, 1976; Quansah, 1981; Poesen, 1985; Grosh and Jarrett, 1994; Kinnell, 2005).

On the other hand, the research on RD–WDT has been gradually building up over the years (Erpul et al., 2002, 2003a, 2004; Cornelis et al., 2004a,b). Fundamentally, these studies are based on RD and WDT partitioning to model the process, and RD–WDT is adequately described by relating it to rainfall impact energy ( $E$ ) and wind shear velocity ( $u_*$ ) (Erpul et al., 2002, 2003a, 2004; Cornelis et al., 2004a,b):

$$q_{RD-WDT} = k_{RD-WDT} [f(E)][f(u_*)] \quad (2)$$

where  $q_{RD-WDT}$  is the amount of material transported by RD–WDT,  $k_{RD-WDT}$  is the soil erodibility associated by RD–WDT and represents confounded reaction of soil to both detachment by wind-driven raindrops and transport by wind, and  $f(E)$  and  $f(u_*)$  are functions that change with the rainfall energy and wind shear velocity, respectively. Using the flux of rain energy based on the normal velocity of wind-driven raindrop impact ( $E_{tz}$ , in J m<sup>-2</sup> s<sup>-1</sup>) and wind shear

velocity ( $u_*$ , m s<sup>-1</sup>), Erpul et al. (2003a) defined the process by following equation:

$$q_{RD-WDT} = 119.95(E_{tz})^{0.81} u_*^{2.09}. \quad (3)$$

They observed that empirically determined constants “0.81” and “2.09” were statistically indifferent from 1.00 and 2.00, respectively for silt loam and loam soils of Belgium. Instead of the resultant energy flux of the wind-driven rains ( $E_t$ ),  $E_{tz}$  was used since the latter resulted better in modeling than the former. Additionally, Cornelis et al. (2004a,b) conducted similar experimentation with very well sorted dune sand collected from the Belgian coast, and they related the raindrop detachment ( $D_{RD}$ ) to  $(E_{tz} - E_{tzt})^a$  instead of  $(E_{tz})^a$ , where  $E_{tzt}$  is the threshold kinetic energy to dislodge sand grains, and the wind transport ( $q_{WDT}$ ) to  $(u_*)^b$ .  $E_{tzt}$  was also derived from the normal velocity of wind-driven raindrop impact as an intercept of the linear curve of sand splash and energy relationship (Sharma and Gupta, 1989). The average values of parameters were 1.0 and 0.41 for “a” and “b”, respectively, for very well sorted dune sand collected from the Belgian coast (Cornelis et al., 2004a).

Although  $E_{tz}$  was directly related to the detachment rates to model RD in both soil and sand transport studies by RD–WDT, Erpul et al. (2005) showed that the tangential stress resulted from the lateral jetting of raindrops had a greater correlation with sand detachment than the compressive stress related to the normal component of the raindrop impact in studies of the sand detachment by wind-driven rain. Later, Erpul et al. (2008) found a relationship between  $D_{RD}$  (g m<sup>-2</sup> s<sup>-1</sup>) and both  $E_{tz}$  and  $E_{tx}$  (J m<sup>-2</sup> s<sup>-1</sup>), where  $E_{tx}$  is the flux of rain energy based on the horizontal velocity of wind-driven raindrop impact:

$$D_{RD} = k_{RD}(E_{tz})^{a_1}(E_{tx})^{a_2} \quad (4)$$

where,  $k_{RD}$  is the soil erodibility associated by RD of wind-driven raindrops. Observed values of constants  $a_1$  and  $a_2$  were 0.83 and 0.87, respectively. Explicitly,  $E_{tx}$  was as good as  $E_{tz}$  at the process of RD in contradiction to the fact that  $D_{RD}$  varied only with the normal component of impact velocity (Ellison, 1947; Heymann, 1967; Springer,

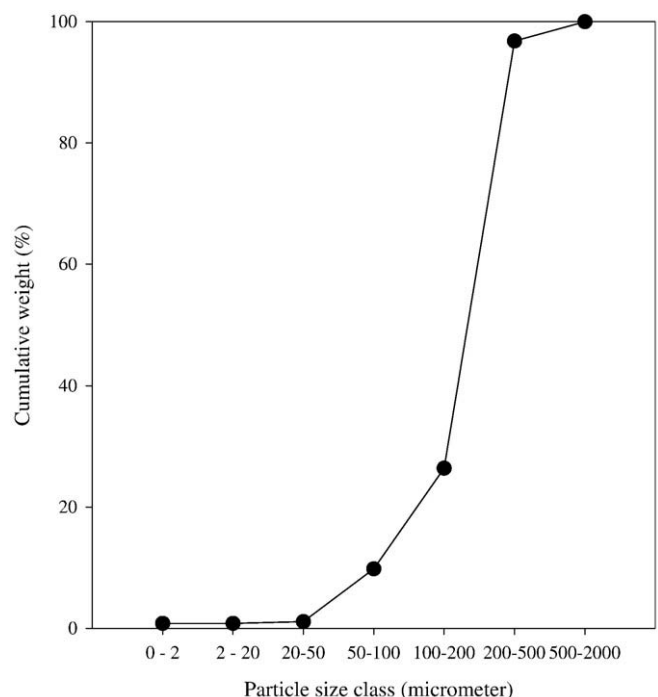


Fig. 1. Cumulative grain size distribution of the sand used in the RD–WDT experiments.

1976; Gilley et al., 1985; Gilley and Finkner, 1985; Erpul et al., 2002, 2003b, 2004; Cornelis et al., 2004a,b). Therefore, this article is specifically intended to quantify the effect of the components of compressive and shear stresses (Huang et al., 1982, 1983; Al-Durrah and Bradford, 1982; Cruse et al., 2000; Erpul et al., 2005, 2008) of obliquely striking wind-driven raindrops on sand detachment to model RD-WDT. The role of these two stress components in entraining sand particles into the splash droplets to be subsequently traveled with the wind is presented in this article.

## 2. Materials and methods

### 2.1. Experimental set-up

RD-WDT experiments were performed under laboratory conditions in the wind tunnel rainfall simulator facility of the International

Center for Eremology, Ghent University, Belgium. The details of the wind tunnel were given by Gabriels et al. (1997), and it was complementarily detailed by Cornelis et al. (2004c), additionally including particulars of the drop size distribution, intensity, and energy of the wind-driven rains of the wind tunnel simulator. In the study, a continuous spraying system of ten downward-oriented nozzles simulated rainfalls at the same time as horizontal wind velocities of 6.4, 10, and 12 m s<sup>-1</sup> passed through the tunnel. Three operating nozzle pressures (75, 100, and 150 kPa) were applied to have different rainfall intensities of the wind-driven rains (Erpul et al., 1998). Tap water was used with an electrical conductivity at 25 °C of 0.7 dS m<sup>-1</sup> since dispersion could be ignored. The sand used in this study was very well sorted dune sand, the cumulative grain size distribution of which is given by Fig. 1, collected from the Belgian coast and its geometric mean particle diameter was 250 μm; calcium carbonate and organic matter content were 3.34% and 0%, respectively.

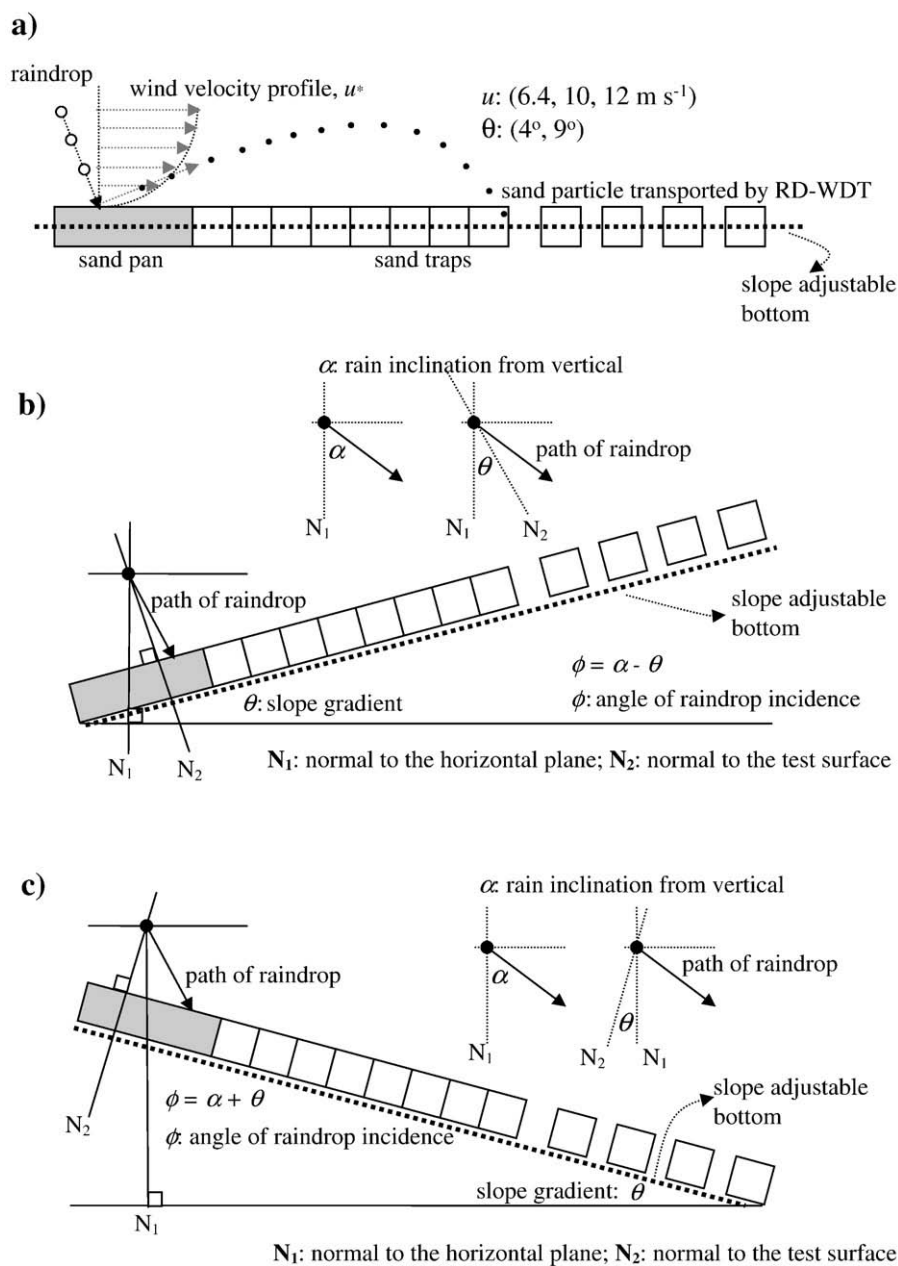
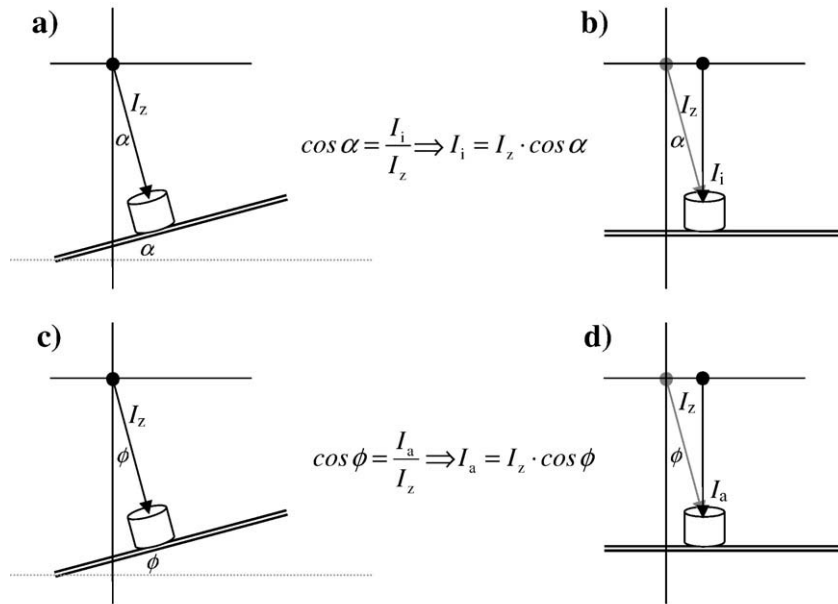


Fig. 2. Experimental set-up with sand pan and traps for RD-WDT (a) plan view, (b) side view of windward set-up, and (c) side view of leeward set-up.



$I_z$ : Intensity with respect to a plane normal to the rain vector  
 $I_i$ : Intensity of inclined rainfall related to the normal component of  $I_z$   
 $I_a$ : Intensity of rain with a given angle of incidence as the normal component of  $I_z$

Fig. 3. Inclined rain intensity measurements ( $I_i$ ) on the horizontal plane (a, b) (Erpul, 1996) and the calculation of the actual rain intensity ( $I_a$ ) from  $I_i$  values under a given angle of incidence (c, d).

The electrical conductivity of the sand was  $0.72 \text{ dS m}^{-1}$  at  $25 \text{ }^\circ\text{C}$  and the bulk density was  $1.7 \text{ Mg m}^{-3}$  (Cornelis et al., 2004a,b).

The sand was placed into a 55-cm long and 20-cm wide pan with a perforated bottom to allow free drainage, and it was located at a distance  $x=6.45 \text{ m}$  downwind from the entrance of the wind tunnel working section along its centerline with both windward and leeward slopes of 7% and 16% ( $4.0^\circ$  and  $9.0^\circ$ , respectively) (Fig. 2). Each rainfall was performed on a pre-wetted sand surface to prevent sand from lifting off due to the wind. The surface was pre-wetted by spraying before it was exposed to the wind-driven rain and smoothed exactly to a level even with the rim of the pan. Accordingly, there was only raindrop-induced, no wind-induced, particle entrainment in the experiment. With three nozzle pressures, three wind velocities, two slope-gradients, two slope-aspects, and two replicates, a total of 72 wind-driven rainfall simulations were performed.

### 2.2. Incidence angle and intensity of wind-driven rain

For wind-driven rain intensity, the actual amount of rain intercepted by the sloping surface (Sharon, 1970, 1980; Sharon et al., 1983, 1988; De Lima, 1990; Sharon and Arazi, 1997; Blocken and Carmeliet, 2000, 2002, 2004; Cornelis et al., 2004c; Blocken et al., 2006) at both

windward and leeward slopes of  $4.0^\circ$  and  $9.0^\circ$  was calculated from the measured wind-driven rain intensities on a horizontal plane for the nozzle operating pressures of 75, 100, and 150 kPa and the horizontal wind velocities of 6.4, 10, and  $12 \text{ m s}^{-1}$  (Erpul, 1996; Erpul et al., 1998, 2000) by the following equations. (Fig. 3):

$$\cos \alpha = I_i / I_z \tag{5}$$

$$\cos \phi = I_a / I_z \tag{6}$$

$$I_i / \cos \alpha = I_a / \cos \phi \Rightarrow I_a = (I_i / \cos \alpha) \cdot (\cos \phi) \tag{7}$$

$$I_i \cdot (\cos(\alpha \pm \theta) / \cos \alpha) = I_i \cdot (\cos \alpha \cdot \cos \theta \pm \sin \alpha \cdot \sin \theta / \cos \alpha) \tag{8}$$

$$I_a = I_i \cdot (\cos \theta \pm \tan \alpha \cdot \sin \theta) \tag{9}$$

where,  $\alpha$ ,  $\theta$ , and  $\phi$  are the raindrop inclination from vertical, slope gradient, and angle of rain incidence; respectively, and  $I_z$ ,  $I_i$ , and  $I_a$  are the intensity with respect to a plane normal to the rain vector (Fig. 3a), intensity of wind-driven rainfall related to the normal component of  $I_z$  (Fig. 3b), and intensity of rain with a given angle of incidence as the normal component of  $I_z$  (Fig. 3c,d), respectively.

$\alpha$  values of the rains driven by the wind velocities of 6.4, 10.0, and  $12.0 \text{ m s}^{-1}$  were  $55^\circ$ ,  $68^\circ$ , and  $72^\circ$ , respectively (Erpul et al., 2005) (Fig. 4).  $\phi$  values of the rains changed with the rain inclination, slope

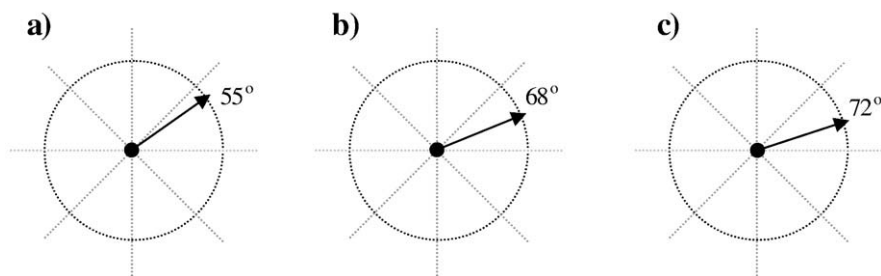
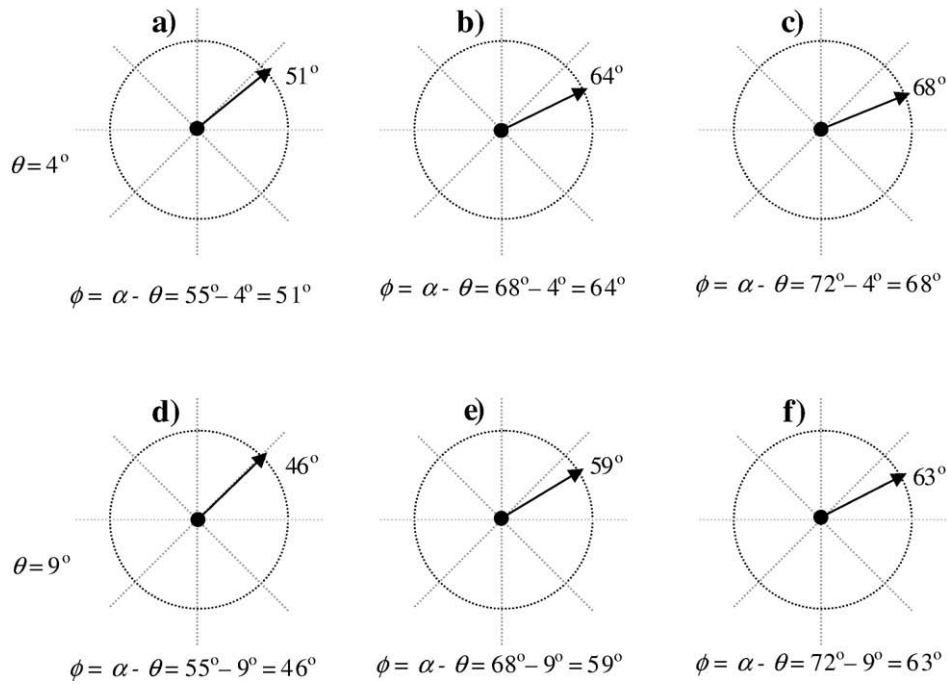


Fig. 4. The inclination of rains ( $\alpha$ ) driven by the wind velocities of 6.4 (a), 10.0 (b), and  $12.0 \text{ m s}^{-1}$  (c).



**Fig. 5.** The angle of rains incident on the sand test surface placed at windward slopes (Ww) of  $4.0^\circ$  (a–c) and  $9.0^\circ$  (d–f) and driven by the wind velocities of  $6.4$  (a, d),  $10.0$  (b, e), and  $12.0 \text{ m s}^{-1}$  (c, f) ( $\phi = \alpha - \theta$ ).

gradient and slope aspect (Figs. 5 and 6). While Fig. 5 shows the angle of the incident rain on the sand test surface placed at the windward slopes of  $4.0^\circ$  and  $9.0^\circ$  and driven by the wind velocities of  $6.4$ ,  $10.0$ , and  $12.0 \text{ m s}^{-1}$ , Fig. 6 illustrates those at the leeward slopes of  $4.0^\circ$  and  $9.0^\circ$  and driven by the same wind velocities.  $\phi$  values of the former were  $51^\circ$ ,  $64^\circ$  and  $68^\circ$ , and  $46^\circ$ ,  $59^\circ$  and  $63^\circ$ , respectively for slopes of  $4.0^\circ$  and  $9.0^\circ$ , and those of the latter were  $59^\circ$ ,  $72^\circ$  and  $76^\circ$ , and  $64^\circ$ ,  $77^\circ$  and  $81^\circ$ , respectively for slopes of  $4.0^\circ$  and  $9.0^\circ$ .

### 2.3. Impact velocity of wind-driven raindrop

Partition of the resultant impact velocity of the wind-driven raindrop ( $v_t$ ) into horizontal ( $v_x$ ) and vertical ( $v_z$ ) components is directly related to the  $\phi$  value by  $v_x = v_t \cdot \sin \phi$  and  $v_z = v_t \cdot \cos \phi$ , respectively (Erpul et al., 2005, 2008). Figs. 4–6 signify the degree of the variation in the lateral jetting of the raindrops associated with  $v_x$  in the experiments. For a given median size ( $d_{50}$ ) ( $1.63$ ,  $1.53$ , and

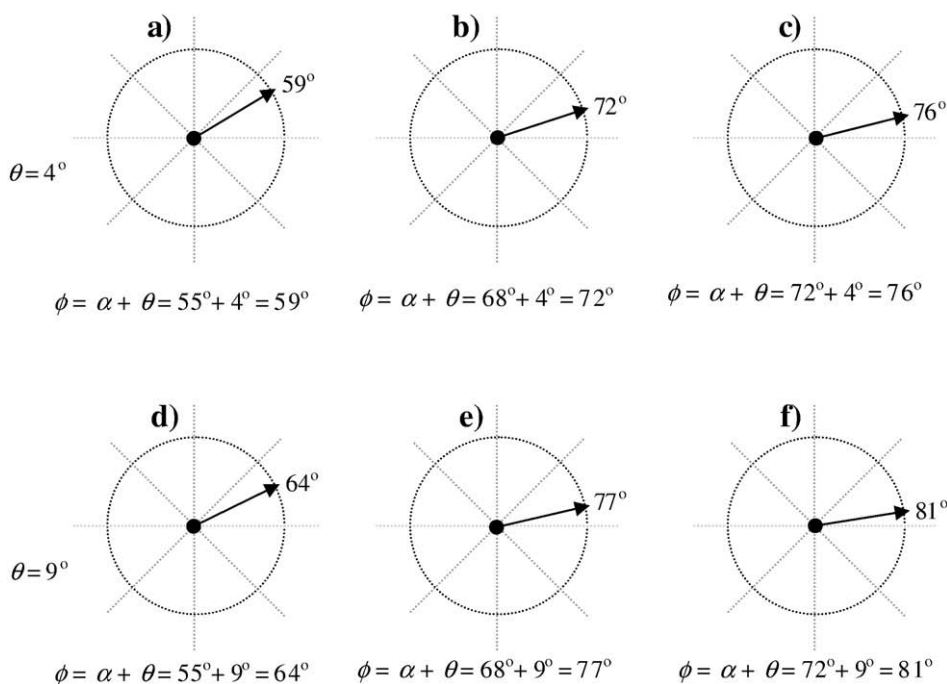


**Fig. 6.** The angle of rains incident on the sand test surface placed at leeward slopes (Lw) of  $4.0^\circ$  (a, b, c) and  $9.0^\circ$  (d, e, f) and driven by the wind velocities of  $6.4$  (a, d),  $10.0$  (b, e), and  $12.0 \text{ m s}^{-1}$  (c, f) ( $\phi = \alpha + \theta$ ).

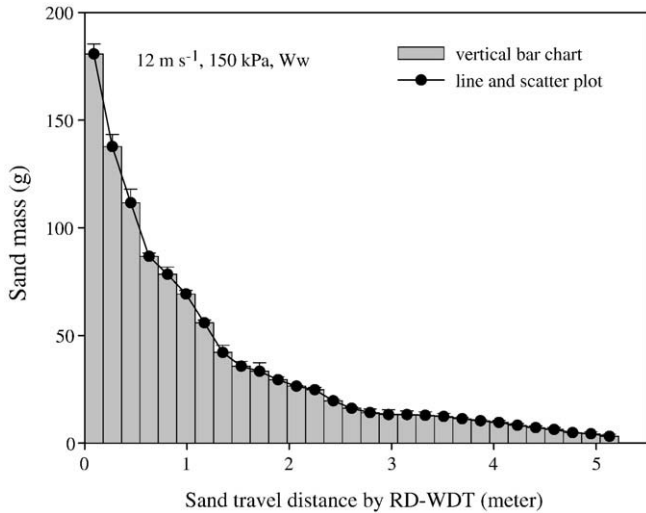


**Fig. 7.** Sample mass distribution of sand particles (g) with travel distance (m) acquired in the rain simulated with 12 m s<sup>-1</sup> wind and 150 kPa nozzle operating pressure and incident on the windward slope (Ww) of 4°.

1.55 mm for the rains driven by 6.4, 10.0, and 12.0 m s<sup>-1</sup> horizontal winds, respectively; Erpul et al., 1998, 2000), v<sub>t</sub> of wind-driven raindrops (m s<sup>-1</sup>) is given as an exponential function of the horizontal wind velocity (u, m s<sup>-1</sup>) (Erpul, 2001):

$$v_t = ce^{d(u)} \quad (10)$$

Corresponding resultant kinetic energy flux (J m<sup>-2</sup> s<sup>-1</sup>) is estimated by:

$$E_t = M[f(v_t)][f(\eta_a)] \quad (11)$$

where M is equal to 0.5 (m) for a given mass (m, kg) of a median raindrop size, and η<sub>a</sub> is in raindrop numbers per unit surface area of sand pan per unit time as a function of I<sub>a</sub> (m<sup>-2</sup> s<sup>-1</sup>). The horizontal and vertical kinetic energy fluxes (E<sub>tx</sub> and E<sub>tz</sub> in J m<sup>-2</sup> s<sup>-1</sup>, respectively) are computed as E<sub>t</sub> · sin<sup>2</sup> φ and E<sub>t</sub> · cos<sup>2</sup> φ, respectively.

#### 2.4. Wind velocity profiles

Wind velocity profiles were measured above the sand pan up to 2 m nozzle height with a vane type anemometer and an associated recording equipment, and characterized by the Prandtl–von Kármán logarithmic equation:

$$u(z) = (u_* / \kappa) \cdot \ln(z/z_0) \quad \text{for } z < z_0 \quad (12)$$

where u(z) is the wind speed at height z, z<sub>0</sub> is the aerodynamic roughness height, u\* is the wind shear velocity, and κ is the von Kármán's constant. The boundary layer was set at 0.3 m above the soil tray, and the resulted aerodynamic roughness height was 0.0006 m. Subsequently, “u\*” for 6.4, 10.0, and 12.0 m s<sup>-1</sup> horizontal winds was derived from Eq. (12). Average wind velocity profiles did not vary with slope gradient but aspect since the experimental set-up with sand pan and traps for RD–WDT changed with aspect (Fig. 2). For 6.4, 10.0, and 12.0 m s<sup>-1</sup> horizontal winds and with the constant “z<sub>0</sub>” of 0.0006, “κ/u\*” values were 0.75, 0.62, and 0.53 in the windward set-up and 1.18, 0.77 and 0.65 in the leeward set-up, respectively, and, in that order, these resulted in u\* (m s<sup>-1</sup>) values of 0.53, 0.65 and 0.76, and 0.34, 0.52 and 0.62.

#### 2.5. Evaluation of sand transport rates

Sand transport rates (q, g m<sup>-1</sup> min<sup>-1</sup>) by RD–WDT were evaluated by the amount of wind-driven sand particles trapped at set distances on a 7-m uniform slope segment. Troughs were placed in upslope and downslope direction, respectively, for windward and leeward slopes of 4.0° and 9.0° (Fig. 2b,c). The sand particles trapped in the collecting troughs were washed, oven-dried, and weighed, and mass distribution of sand particles with travel distance (x, m) was acquired for each run (Fig. 7). These were afterward used to produce exponential decay curves, and exponentially fitted curves with parameter values (β and σ coefficients that depended upon the physical properties of sand particles) were integrated over RD–WDT distance to determine q (Savat and Poesen, 1981; Poesen, 1985; Wright, 1987; Van Dijk et al., 2002; Mouzai and Bouhadef, 2003; Erpul et al., 2003a, 2004; Leguëdois et al., 2005; Legout et al., 2005; Furbish et al., 2007).

$$q = (\beta/At) \int e^{-\sigma x} dx \quad (13)$$

where, A = the collecting trap area (in our case 0.168 m<sup>2</sup> with a length of 1.20 m and width of 0.14 m), and t = time of sampling (45 min).

**Table 1**  
Angle of rain incidences and intensities of simulated wind-driven rainfalls with 6.4, 10, and 12 m s<sup>-1</sup> horizontal winds under different nozzle operating pressures

u (m s <sup>-1</sup> )	α (°)	θ (°)	P (kPa)	d <sub>50</sub> (mm)	Windward						Leeward					
					u*	I <sub>a</sub>	η <sub>a</sub>	φ (°)	sin φ	cos φ	u*	I <sub>a</sub>	η <sub>a</sub>	φ (°)	sin φ	cos φ
6.4	55	4.0	75	1.62	0.53	125	1.54E+04	51	0.7771	0.6293	0.34	102	1.28E+04	59	0.8572	0.5150
			100	1.58		128	1.71E+04					105	1.42E+04			
			150	1.63		136	1.66E+04					112	1.38E+04			
	9.0	75	1.64	0.53	139	1.71E+04	46	0.7193	0.6947	0.34	87	1.11E+04	64	0.8988	0.4384	
		100	1.67		143	1.90E+04					90	1.23E+04				
		150	1.52		152	1.84E+04					96	1.20E+04				
10.0	68	4.0	75	1.61	0.65	127	1.53E+04	64	0.8988	0.4384	0.52	89	1.07E+04	72	0.9511	0.3090
			100	1.53		130	1.48E+04					92	1.04E+04			
			150	1.55		160	2.42E+04					113	1.70E+04			
	9.0	75	1.62	0.65	151	1.82E+04	59	0.8572	0.5150	0.52	65	7.79E+03	77	0.9744	0.2250	
		100	1.58		155	1.77E+04					67	7.58E+03				
		150	1.63		191	2.89E+04					83	1.24E+04				
12.0	72	4.0	75	1.64	0.76	134	1.72E+04	68	0.9272	0.3746	0.62	86	1.08E+04	76	0.9703	0.2419
			100	1.67		140	2.10E+04					91	1.32E+04			
			150	1.52		169	2.43E+04					109	1.53E+04			
	9.0	75	1.61	0.76	164	2.13E+04	63	0.8910	0.4540	0.62	56	6.67E+03	81	0.9877	0.1564	
		100	1.53		172	2.60E+04					59	8.15E+03				
		150	1.55		208	3.02E+04					71	9.45E+03				

u: horizontal wind velocity (m s<sup>-1</sup>); α: rain inclination from vertical (°); θ: slope gradient (°); P: nozzle operating pressures (kPa); d<sub>50</sub>: median drop size (mm); u\*: wind shear velocity (m s<sup>-1</sup>); I<sub>a</sub>: actual rainfall intensity (mm h<sup>-1</sup>); η<sub>a</sub>: number of raindrop (# m<sup>-2</sup> s<sup>-1</sup>); φ: angle of rainfall incidence (°), φ = [α - θ] for windward and φ = [α + θ] for leeward.

Finally,  $q$  by the process RD–WDT ( $q_{RD-WDT}$ ) was described as a non-linear function of  $E_{tz}$ ,  $E_{tx}$ , and  $u_*$ :

$$q_{RD-WDT} = k_{RD-WDT}(E_{tz})^{\chi_1}(E_{tx})^{\chi_2}u_*^{\chi_3} \quad (14)$$

where,  $k_{RD-WDT}$  is the soil erodibility associated by RD–WDT, and “ $\chi_1$ ”, “ $\chi_2$ ”, and “ $\chi_3$ ” were the model parameter values that showed the effectiveness of raindrop compressive stress, raindrop shear stress, and wind shear velocity on RD–WDT, respectively.

### 3. Results and discussion

Angle of rain incidences and intensities of the simulated wind-driven rainfalls with 6.4, 10, and 12 m s<sup>-1</sup> horizontal winds under nozzle operating pressures of 75, 100, and 150 kPa are given in Table 1. Figs. 5 and 6 give  $\phi$  values as a function of rain inclination ( $\alpha$ , °), slope gradient ( $\theta$ , °) and slope aspect, for which positive and negative sign of  $\theta$  is used for windward and leeward slopes, respectively, in order to show that different  $\phi$  values occur with the same values of  $\alpha$  and  $\theta$  (Fig. 2). Noticeably, for each  $u$  level, by changing slope aspect and  $\theta$ , different values of  $\phi$  were acquired relative to  $\alpha$  values (Table 1 and Figs. 5 and 6). Variations in  $\phi$  resulted in an opportunity of working with different fluxes of rain energies based on both normal and horizontal velocities of wind-

driven raindrop impact ( $E_{tz}$  and  $E_{tx}$ , J m<sup>-2</sup> s<sup>-1</sup>) as they were directly a function of  $\phi$ . The bounds of  $\phi$  and its normal and horizontal components ( $\cos \phi$ , and  $\sin \phi$ , respectively) were  $46 \leq \phi \leq 81^\circ$ ,  $0.16 \leq \cos \phi \leq 0.69$ , and  $0.78 \leq \sin \phi \leq 0.99$ , respectively. Since  $E_{tz}$  and  $E_{tx}$ , varied respectively with  $\cos \phi$  and  $\sin \phi$ ,  $E_{tz}$  attained a low value of 0.16 and  $E_{tx}$  a high value of 0.99 (Table 1).

Fig. 8 shows  $I_a$  values of the simulated wind-driven rainfalls as influenced by  $\phi$  and  $P$ . Upper and lower bounds of the vertical axis in Fig. 8 were set as the highest and lowest  $I_a$  values to display variations in  $I_a$  with  $\phi$  and  $P$ . Together with wide ranges of  $\phi$ , different  $I_a$  values ( $208 \leq I_a \leq 56$  mm h<sup>-1</sup>) let the RD–WDT experiments be performed with broad combinations of  $E_{tz}$  and  $E_{tx}$  although their vectored sum ( $E_t$ , J m<sup>-2</sup> s<sup>-1</sup>) was similar for some cases (Table 2 and Fig. 9).

$E_t$  increased as  $u$  increased at each level of  $P$ , and for a particular  $u$ ,  $E_t$  was greater in the windward slopes than in the leeward slopes as  $I_a$  values were greater in the former case (Table 1, Figs. 8 and 9). Fig. 9 also shows the magnitude of  $E_{tx}$  and  $E_{tz}$ . There was more noticeable  $E_{tz}$  contribution to  $E_t$  in the windward slopes than in the leeward slopes compared to that of  $E_{tx}$ , although for the most part,  $E_{tx}$  was much greater than  $E_{tz}$ , and RD–WDT was measured with the improved description of lateral jets of the wind-driven raindrops (Table 2 and Fig. 9). In other terms,  $E_{tx}$  appeared to have more control over RD than  $E_{tz}$  in magnitude, and with this, the study differed from those previously carried out and only considered  $E_{tz}$  in RD.

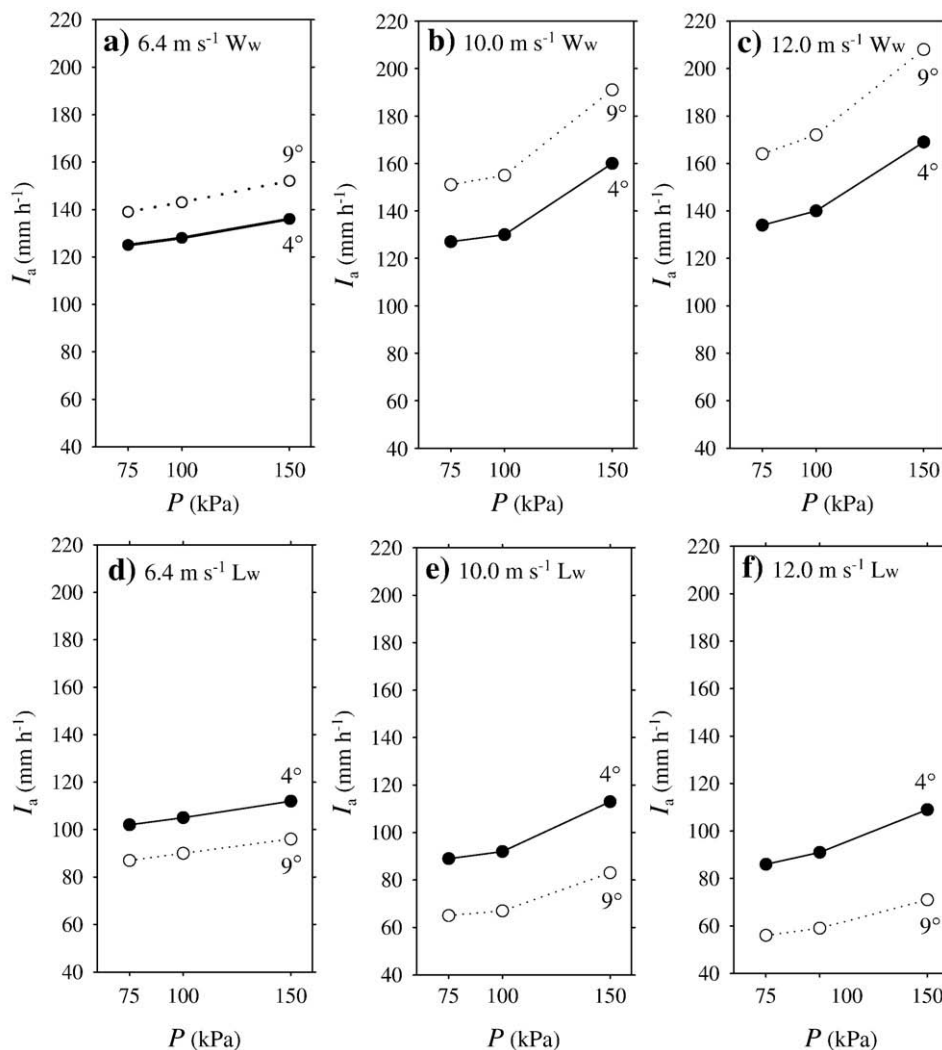


Fig. 8. Actual intensity values ( $I_a$ , mm h<sup>-1</sup>) of the simulated wind-driven rainfalls as influenced by angle of rain incidence ( $\phi = \alpha + \theta$ ) and nozzle operating pressure ( $P$ , kPa).

**Table 2**  
Resultant total energy flux and its components and measured sand transport rate by RD–WDT for the simulated rains with horizontal winds of 6.4, 10.0, and 12.0 m s<sup>-1</sup> and nozzle operating pressures of 75, 100, and 150 kPa

<i>u</i> (m s <sup>-1</sup> )	$\alpha$ (°)	$\theta$ (°)	<i>P</i> (kPa)	Winward				Leeward							
				<i>E<sub>t</sub></i>	<i>E<sub>tz</sub></i>	<i>E<sub>tx</sub></i>	<i>n</i>	<i>q<sub>m(RD-WDT)</sub></i>		<i>E<sub>t</sub></i>	<i>E<sub>tz</sub></i>	<i>E<sub>tx</sub></i>	<i>n</i>	<i>q<sub>m(RD-WDT)</sub></i>	
				(J m <sup>-2</sup> s <sup>-1</sup> )	(J m <sup>-2</sup> s <sup>-1</sup> )	(J m <sup>-2</sup> s <sup>-1</sup> )		(g m <sup>-1</sup> min <sup>-1</sup> )	Mean	SD	(J m <sup>-2</sup> s <sup>-1</sup> )	(J m <sup>-2</sup> s <sup>-1</sup> )		(J m <sup>-2</sup> s <sup>-1</sup> )	(g m <sup>-1</sup> min <sup>-1</sup> )
6.4	55	4.0	75	0.344	0.148	0.196	2	4.17	0.17	0.285	0.085	0.201	2	2.40	0.01
			100	0.381	0.164	0.217	2	7.40	0.10	0.316	0.094	0.222	2	2.88	0.23
			150	0.369	0.159	0.210	2	7.71	1.94	0.307	0.091	0.216	2	3.19	0.86
		9.0	75	0.381	0.198	0.183	2	4.44	0.09	0.248	0.054	0.193	2	1.95	0.01
			100	0.422	0.219	0.203	2	5.66	0.78	0.274	0.060	0.214	2	3.68	0.23
			150	0.410	0.213	0.197	2	5.36	0.76	0.266	0.058	0.208	2	2.34	0.52
10.0	68	4.0	75	0.813	0.154	0.659	2	22.93	0.14	0.571	0.053	0.518	2	6.95	0.65
			100	0.791	0.150	0.641	2	25.25	0.98	0.555	0.052	0.504	2	5.51	0.04
			150	1.292	0.245	1.047	2	27.46	2.61	0.907	0.085	0.823	2	13.99	0.25
		9.0	75	0.969	0.255	0.714	2	27.09	0.35	0.415	0.020	0.395	2	3.14	0.13
			100	0.942	0.248	0.694	2	29.59	0.27	0.404	0.020	0.384	2	3.52	0.16
			150	1.540	0.406	1.134	2	26.54	1.43	0.660	0.032	0.628	2	6.54	0.77
12.0	72	4.0	75	1.417	0.174	1.243	2	29.80	1.12	0.890	0.042	0.848	2	15.71	1.14
			100	1.732	0.212	1.520	2	25.98	1.02	1.087	0.051	1.036	2	15.17	0.13
			150	2.008	0.246	1.762	2	27.58	1.49	1.261	0.059	1.202	2	16.80	0.45
		9.0	75	1.757	0.328	1.429	2	39.51	0.77	0.550	0.009	0.541	2	3.10	0.77
			100	2.148	0.401	1.747	2	28.20	0.50	0.672	0.011	0.661	2	6.37	4.30
			150	2.490	0.465	2.025	2	30.91	0.81	0.779	0.013	0.766	2	14.45	1.12

*u*: horizontal wind velocity;  $\alpha$ : rain inclination from vertical;  $\theta$ : slope gradient; *E<sub>t</sub>*: total resultant energy flux; *E<sub>tz</sub>*: energy flux calculated using vertical component of impact velocity; *E<sub>tx</sub>*: energy flux calculated using horizontal component of impact velocity; *q<sub>m(RD-WDT)</sub>*: measured sand transport rate by RD–WDT; SD: standard deviation; *n*: replicate.

Measured sand transport rates by RD–WDT (= *q<sub>m(RD-WDT)</sub>*) are given in Table 2. Bar graphs of *q<sub>m(RD-WDT)</sub>* values versus horizontal wind velocity (*u*) at each slope gradient and aspect and versus angle of rain incidence ( $\phi$ ) at each wind velocity are presented in Fig. 10a and b, respectively. This was irrespective of nozzle operating pressures (*P*) since *P* effect on *q<sub>m(RD-WDT)</sub>* was indistinct and neither increasing nor decreasing *q<sub>m(RD-WDT)</sub>* patterns were observed as nozzle operating pressure changed. On the other hand, at the each slope gradient and aspect, the sand transport rate increased as the wind velocity increased (Fig. 10a), and at each wind velocity, it decreased as the angle of the wind-driven rain incidence increased (Fig. 10b). The former was because wind-driven raindrops gained a degree of horizontal velocity, which subsequently increased their resultant impact velocity and energy. A preceding study, performed for sand detachment from splash cups, showed that the kinetic energy flux calculated by the resultant impact velocity of wind-driven raindrops adequately described the rates (Erpul et al., 2005). Whereas, the latter was because increase in  $\phi$  values resulted in a decrease in intensity ( $I_a = I_z \cos \phi$ ) and normal velocity of the wind-driven rains ( $v_z = v_z \cos \phi$ ). Van Heerden (1964) found that sand detachment decreased under wind-driven rains with appreciable angle of incidences although the detached particles traveled greater distances since wind acted as a transporting agent, and Huang et al. (1982) reported that the compressive pressure build-up at the raindrop–soil interface by normal raindrop impact was directly related to detachment. Also, Fig. 10a shows that, as the slope gradient increased from 4° to 9°, the greater and lower *q<sub>m(RD-WDT)</sub>* values were observed in the windward (*W<sub>w</sub>*) and leeward (*L<sub>w</sub>*) slopes, respectively. Similarly, the reason for this was the fact that there was decrease in *I<sub>a</sub>* and *E<sub>tz</sub>* with increasing  $\phi$  since the slope gradient acted inversely on  $\phi$  to the way which its increment for a particular value of *u* or  $\alpha$  respectively decreased and increased  $\phi$  in *W<sub>w</sub>* and *L<sub>w</sub>*.

Individual scatter plots of *q<sub>m(RD-WDT)</sub>* against *E<sub>t</sub>*, *E<sub>tz</sub>*, *E<sub>tx</sub>*, and *u\**, and each fitted with a linear line, are shown in Fig. 11a–d, respectively. The lines are for prediction to indicate a trend in the data. Fig. 11a shows that the data clustered around the line more tightly at the higher values of *u\** and were more scattered away from the line with greater deviations at lower values, signifying a clearer effect of *u\** on *q<sub>m(RD-WDT)</sub>* in the former case. While there was a good degree of

association between *q<sub>m(RD-WDT)</sub>* and *E<sub>t</sub>* since the amount of scatter above or below the trend line was not very large (Fig. 11b), that between *q<sub>m(RD-WDT)</sub>* and *E<sub>tz</sub>* had a very poor relation since the data points had a lot of scatter (Fig. 11c). *E<sub>tz</sub>* had a very narrower interval compared to *E<sub>tx</sub>* ( $0.009 \leq E_{tz} \leq 0.465$  and  $0.193 \leq E_{tx} \leq 2.025$ , J m<sup>-2</sup> s<sup>-1</sup>, respectively) in this study, with the increased lateral jetting of wind-induced raindrops. The data points of Fig. 11c did not show a clear pattern with a tight cluster around the line, and apparently, there was no obvious association between *q<sub>m(RD-WDT)</sub>* and *E<sub>tz</sub>*. However, the strength of association was high between *q<sub>m(RD-WDT)</sub>* and *E<sub>tx</sub>*, and almost the same scatter plot clustering around a straight line as *E<sub>t</sub>* had with *q<sub>m(RD-WDT)</sub>* appeared (Fig. 11d).

Further support for a better interpretation of the results can be seen on a 3D scatter plot of *q<sub>m(RD-WDT)</sub>* versus *E<sub>tz</sub>* and *E<sub>tx</sub>* (Fig. 12a), and combining the scatter data of both with an additional straight line. When Fig. 12a, which accounted for the distinct effect of *E<sub>tz</sub>* and *E<sub>tx</sub>* on *q<sub>m(RD-WDT)</sub>*, was compared with Fig. 11b, which only explained the effect of *E<sub>t</sub>* on *q<sub>m(RD-WDT)</sub>*, a more descriptive clustering appeared in Fig. 12a, extracting potentially useful information from the data set, which was implicit in Fig. 11b. For example, Fig. 12a provided a better visualization of the data at the lower and upper values of *q<sub>m(RD-WDT)</sub>*. Cruse et al. (2000) reported that the relative importance of *E<sub>tz</sub>* and *E<sub>tx</sub>* in soil detachment was indeterminate and on the basis of detachment and transport processes there was a need to determine this for a better erosion prediction technology although the focus was on *E<sub>tz</sub>* in the processes. Under wind-driven rain studies, Erpul et al. (2005, 2008) compared the partial importance of *E<sub>tz</sub>* and *E<sub>tx</sub>* with the importance of *E<sub>t</sub>* by power models and the model of  $k_{RD}(E_{tz})^{a_1}(E_{tx})^{a_2}$  explained more variation in the sand detachment by wind-driven raindrops than that of  $k_{RD}(E_t)^a$  alone.

Log-linear regression analyses for the predicting sand transport rate by RD–WDT (*q<sub>PRD-WDT</sub>*) by the resultant total energy flux (*E<sub>t</sub>*) and wind shear velocity (*u\**) and by the normal and horizontal partitions of *E<sub>t</sub>* (*E<sub>tz</sub>* and *E<sub>tx</sub>*, respectively) and *u\** are presented in Table 3. These statistics showed that the RD–WDT model constructed under the modeling process by physically investigating the distinct effect of *E<sub>tz</sub>* and *E<sub>tx</sub>* on RD together with *u\** led to a better coefficient of determination ( $R^2 = 0.89$ ) than that only *E<sub>t</sub>* did along with *u\** ( $R^2 = 0.84$ ). The latter is graphed by a 3D scatter plot of *q<sub>m(RD-WDT)</sub>* versus *E<sub>t</sub>* and *u\** in

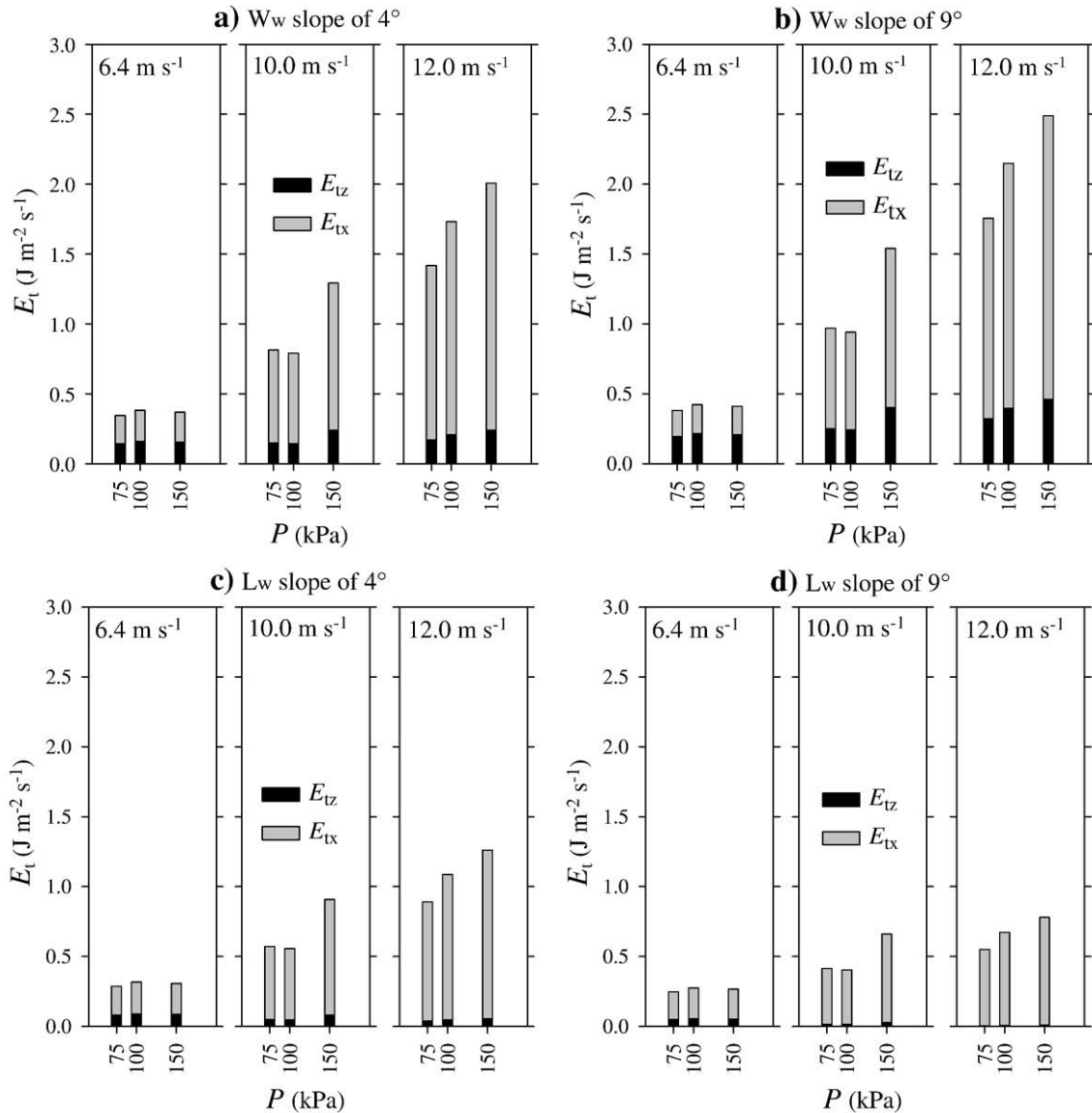


Fig. 9.  $E_t$  ( $J m^{-2} s^{-1}$ ) values with partitions of  $E_{tz}$  ( $J m^{-2} s^{-1}$ ) and  $E_{tx}$  ( $J m^{-2} s^{-1}$ ) for the simulated rainfalls with 6.4, 10, and 12  $m s^{-1}$  horizontal winds under different  $\phi$  and  $P$  values.

Fig. 12b, and a scatter plot of  $q_{m(RD-WDT)}$  versus  $q_{p(RD-WDT)}$  with the model of Eq. (14) given in Fig. 13.

Differentiation of the role of the tangential stress related to  $E_{tx}$  and the compressive stress related to  $E_{tz}$  in RD part of RD-WDT resulted in an apparent improvement to such an extent that  $E_t$ , by itself, could not account for all the variation in entraining sand particles into the splash droplets to be subsequently traveled with the wind. In the model of  $q_{p(RD-WDT)} = (k_{RD-WDT}) E_t^{\delta_1} u_*^{\delta_2}$ , the exponent values to which  $E_t$  and  $u_*$  were raised were 1.03 and 0.77, respectively while the model of  $q_{p(RD-WDT)} = (k_{RD-WDT}) E_{tz}^{\chi_1} E_{tx}^{\chi_2} u_*^{\chi_3}$  produced exponent values of  $\chi_1$ ,  $\chi_2$ , and  $\chi_3$  equal to 0.31, 0.62, and 1.20, respectively. When the results of two models were compared, it appeared that the power of  $E_t$  ( $\delta_1=1.03$ ) was approximately partitioned into 1/3 and 2/3 for  $E_{tz}$  and  $E_{tx}$ , respectively ( $\chi_1=0.31$  and  $\chi_2=0.62$ ) for RD in the latter case, with which there was also an increase for the role of  $u_*$  in the process of WDT ( $\delta_2=0.77$  and  $\chi_3=1.20$ , respectively). Markedly, the partitioning of the resultant energy flux resulted not only in determining distinctive part of each energy component in the sand detachment but also in clearing up the possible inaccuracy in the performance of wind shear velocity in

the sand transport part of RD-WDT. This upgrading was achieved because  $u_*$  exerted a dual function on RD-WDT. One was in RD by changing the magnitude of  $E_{tx}$ , and the second was in WDT as a transporting agent. As a result, the partition of  $E_t$  into  $E_{tz}$  and  $E_{tx}$  caused the model to distinguish the interaction between  $u_*$  and  $E_{tx}$  and to work better (Table 3).

Additionally, Table 4 presents the Pearson correlation coefficients between  $q_{m(RD-WDT)}$  and  $E_t$ ,  $E_{tz}$ ,  $E_{tx}$ , and  $u_*$ . The results showed that  $E_{tx}$  had a better correlation coefficient with  $q_{m(RD-WDT)}$  (0.84) than  $E_{tz}$  (0.55), implying that  $E_{tx}$  and  $E_{tz}$  accounted for 84% and 55% of the variation in  $q_{m(RD-WDT)}$ , respectively, in the experiments of RD-WDT conducted under improved lateral jetting of raindrops induced by wind. The coefficients of  $E_t$  and  $u_*$  with  $q_{m(RD-WDT)}$  were 0.91 and 0.84, respectively.

Huang et al. (1982) showed that the magnitude of the lateral shear stress of a vertically impacting raindrop was straightforwardly correlated to that of the compressive stress, and later, Al-Durrah and Bradford (1982) described the fact how compressive stress was transformed to or compensated by lateral shear stress from the radial splashes. Finally, Huang et al. (1983) explained the lateral jet

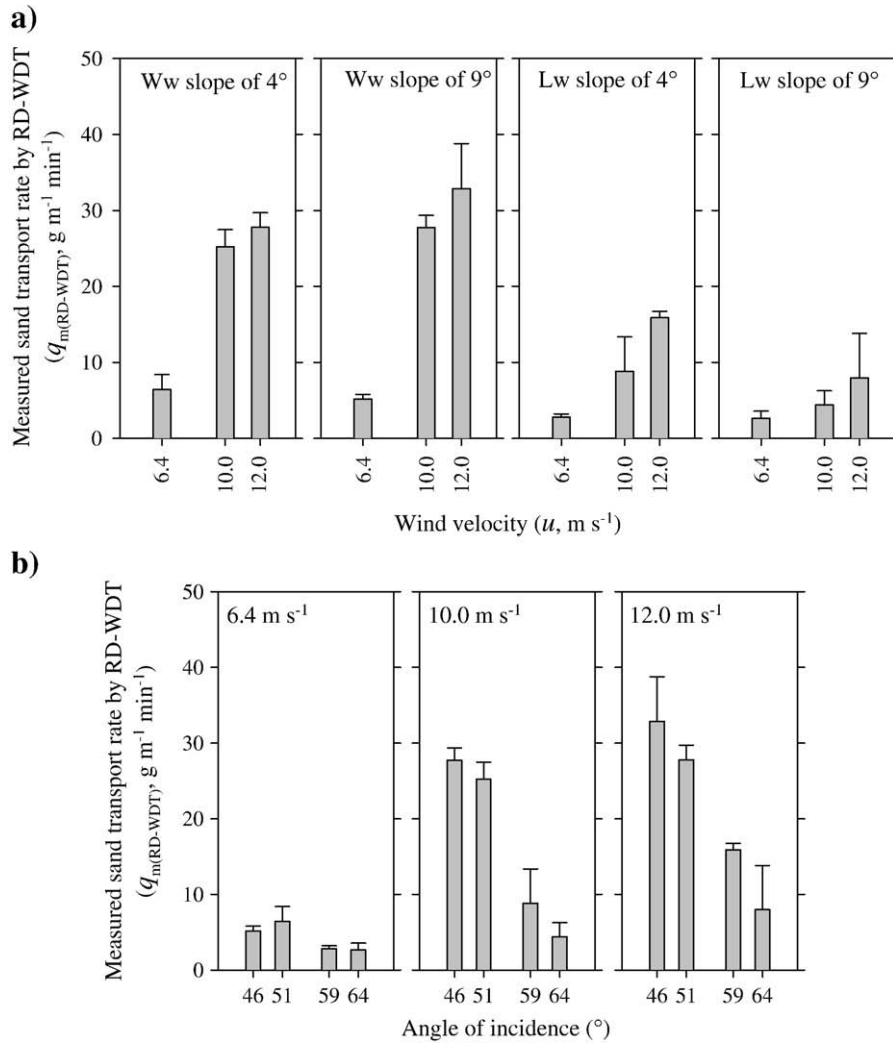


**Fig. 10.** Measured sand transport rate ( $q_{m(RD-WDT)}$ ,  $g m^{-1} min^{-1}$ ) versus wind velocity ( $u$ ,  $m s^{-1}$ ) at each slope gradient and aspect (a) and versus angle of rain incidence ( $\phi$ ,  $^\circ$ ) at each wind velocity (b) regardless of nozzle operating pressures.

development depending on the compressive stress and elasticity or rigidity of rain-impacted surface. Conversely, in this study, there was an insignificant correlation between  $E_{tz}$  and  $E_{tx}$  at the statistical level of  $p=0.05$  (21%), and instead,  $E_{tx}$  was strongly related to  $u^*$  (82%)

(Table 4). At this connection it is reasoned that induced lateral jets by the horizontal wind velocity caused the sand detachment rather than the compensatory lateral jets resulting from the compressive pressure build-up at the raindrop-sand surface.

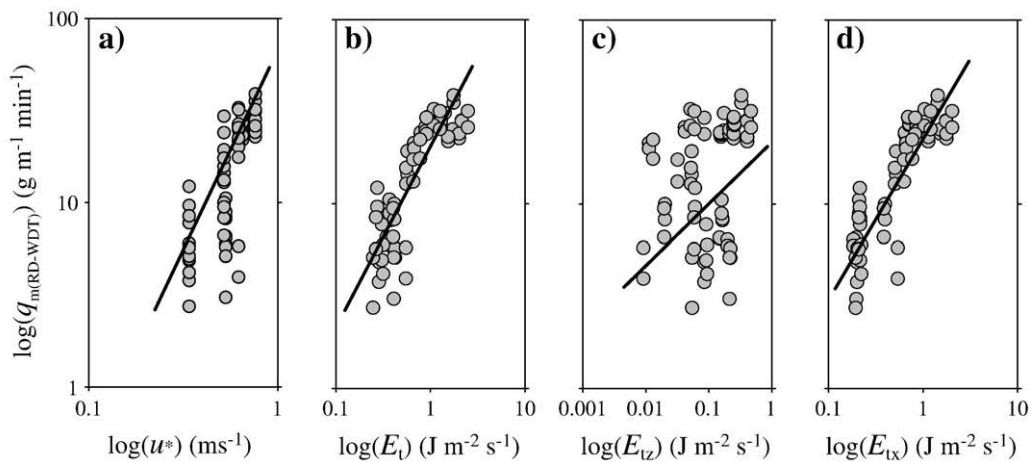


**Fig. 11.** Measured sand transport rates ( $q_{m(RD-WDT)}$ ,  $g m^{-1} min^{-1}$ ) versus  $u^*$  (a),  $E_t$  (b)  $E_{tz}$  (c), and  $E_{tx}$  (d).

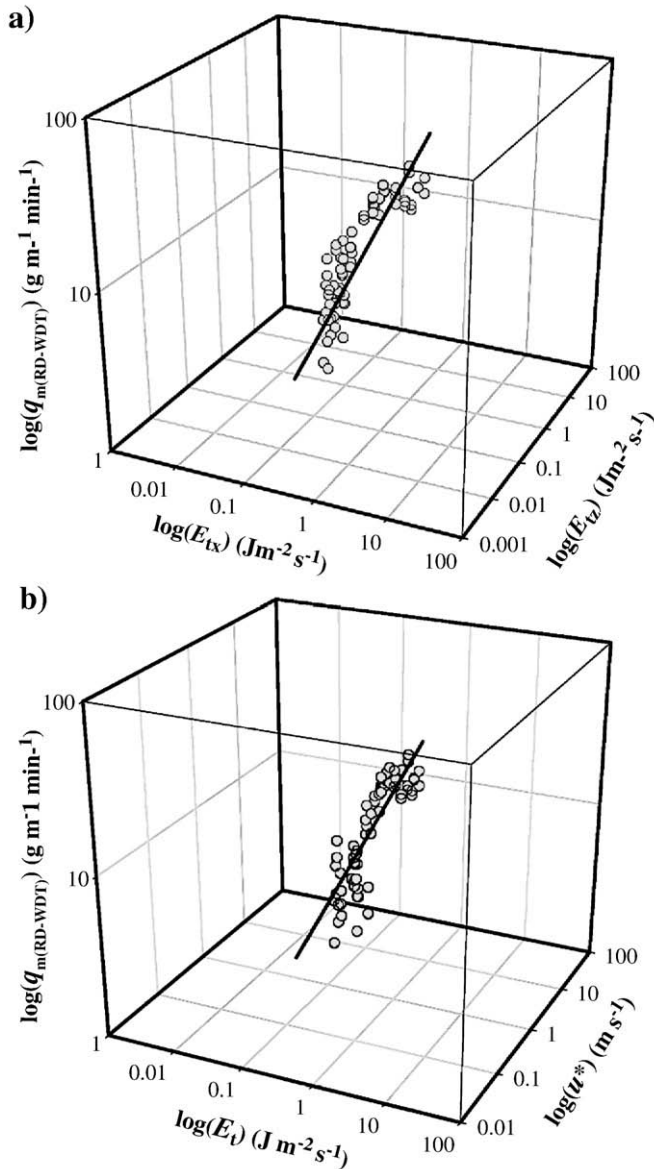


Fig. 12. 3D scatter plot of measured sand transport rate ( $q_{m(RD-WDT)}$ ,  $\text{g m}^{-1} \text{min}^{-1}$ ) versus  $E_{tz}$  and  $E_{tx}$  (a) and  $E_t$  and  $u_*$  (b).

On the other hand, although  $E_{tx}$  was more correlated with  $q_{m(RD-WDT)}$  than  $E_{tz}$ , the results of RD-WDT showed that there was more sand detachment for WDT in the windward slopes (Fig. 10a) where the magnitude of  $E_{tz}$  and  $E_{tx}$  was more comparable (Fig. 9) than that in the leeward slopes where decreases in  $E_{tz}$  were very

Table 3

Statistical analysis for predicting sand transport rate by RD-WDT ( $q_{p(RD-WDT)}$ ,  $\text{g m}^{-1} \text{min}^{-1}$ ) by resultant total energy flux ( $E_t$ ,  $\text{J m}^{-2} \text{s}^{-1}$ ) and wind shear velocity ( $u_*$ ,  $\text{m s}^{-1}$ ) and by normal and horizontal partitions of  $E_t$  ( $E_{tz}$  and  $E_{tx}$ ,  $\text{J m}^{-2} \text{s}^{-1}$ , respectively) and wind shear velocity ( $u_*$ ,  $\text{m s}^{-1}$ ) by log-linear regression

Model	$k_{(RD-WDT)}$	$\delta_1$	$\delta_2$	$R^2$	
$q_{p(RD-WDT)} = (k_{RD-WDT})E_t^{\delta_1} u_*^{\delta_2}$	22.12	1.03	0.77	0.84	
Model	$k_{(RD-WDT)}$	$\chi_1$	$\chi_2$	$\chi_3$	$R^2$
$q_{p(RD-WDT)} = (k_{RD-WDT})E_{tz}^{\chi_1} E_{tx}^{\chi_2} u_*^{\chi_3}$	58.46	0.31	0.62	1.20	0.89

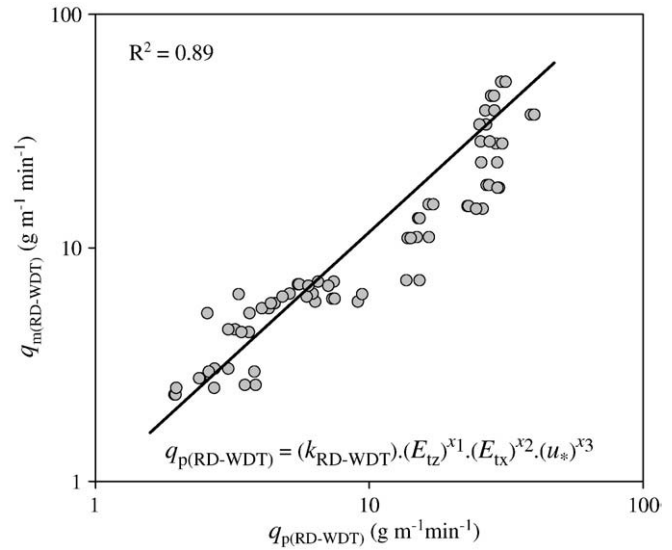


Fig. 13. Scatter plot with a log-linear regression line of measured ( $q_{m(RD-WDT)}$ ,  $\text{g m}^{-1} \text{min}^{-1}$ ) versus predicted sand transport rates ( $q_{p(RD-WDT)}$ ,  $\text{g m}^{-1} \text{min}^{-1}$ ) by RD-WDT.

large (Fig. 9), and thus, extreme increases in  $E_{tx}$  at the expense of  $E_{tz}$  did not bring about significant increases in  $q_{m(RD-WDT)}$ .

4. Conclusions

Sand transport experiments to study the process of RD-WDT were performed under improved lateral jetting of raindrops driven by wind velocities of 6.4, 10, and 12  $\text{m s}^{-1}$  at nozzle operating pressures of 75, 100, and 150 kPa. Obliquely falling wind-driven raindrops were incident to the sand surface on the windward and leeward slopes at 4° and 9°, leading to a wide range in the angle of incidence. The intention of the experiment was to distinguish between the roles of both impact components of obliquely striking wind-driven raindrops on RD and wind on WDT. Raindrop impact components and reference horizontal wind were quantified by normal and horizontal kinetic energy fluxes ( $E_{tz}$  and  $E_{tx}$ , respectively) and wind shear velocity ( $u_*$ ), respectively, to physically model the process. The results showed, at each level of  $u_*$ , differential sand transport rates by RD-WDT ( $q_{m(RD-WDT)}$ ) occurred depending on the magnitude of raindrop impact components, and  $q_m(RD-WDT)$  increased as the relative contribution of  $E_{tz}$  increased. Although  $E_{tx}$  was more correlated with  $q_{m(RD-WDT)}$  (84%) than  $E_{tz}$  (55%), the extreme increases in  $E_{tx}$  at the expense of  $E_{tz}$  cause no increase but a decrease in  $q_{m(RD-WDT)}$ . An RD-WDT model was built by investigating the distinct effects of  $E_{tz}$  and  $E_{tx}$  on RD together with  $u_*$  and resulted in a better coefficient of determination ( $R^2=0.89$ ) than that only  $E_t$  did together with  $u_*$  ( $R^2=0.84$ ). In this study,  $E_{tx}$  was statistically related to  $u_*$  significantly (82%) and not to the  $E_{tz}$  (21%), which was the primary dissimilarity from earlier detachment studies, which depended on the compensatory lateral jet development by

Table 4

Pearson correlation coefficients between the measured sand transport rate ( $q_{m(RD-WDT)}$ ,  $\text{g m}^{-1} \text{min}^{-1}$ ) and  $E_t$ ,  $E_{tz}$ ,  $E_{tx}$ , and  $u_*$

	$E_t$	$E_{tz}$	$E_{tx}$	$u_*$	$q_m$
$E_t$	1.00 (0.0000)	0.42 (0.0003)	0.97 (0.0001)	0.87 (0.0001)	0.91 (0.0001)
$E_{tz}$		1.00 (0.0000)	0.21 (0.0706)	0.32 (0.0067)	0.55 (0.0001)
$E_{tx}$			1.00	0.82 (0.0001)	0.84 (0.0001)
$u_*$				1.00	0.84 (0.0001)
$q_m$					1.00 (0.0000)

the compressive pressure build-up at the raindrop–soil interface. Including  $E_{tx}$  in the RD–WDT model both singled out the distinct role of every raindrop impact component in RD and improved the performance of  $u_*$  in WDT by better describing its interaction with  $E_{tx}$ , which was indistinct in previous models of RD–WDT.

## Acknowledgement

Authors gratefully acknowledge Dr. Takashi Oguchi for his helpful comments during the revision of this manuscript.

## References

- Al-Durrah, M.M., Bradford, J.M., 1982. The mechanism of raindrop splash on soil surfaces. *Soil Science Society of America Journal* 46, 1086–1090.
- Blocken, B., Carmeliet, J., 2000. Driving rain on building envelopes – I: numerical estimation and full-scale experimental verification. *Journal of Thermal Envelope & Building Science* 24, 61–85.
- Blocken, B., Carmeliet, J., 2002. Spatial and temporal distribution of driving rain on a low-rise building. *Wind and Structures* 5, 441–462.
- Blocken, B., Carmeliet, J., 2004. A review of wind-driven rain research in building science. *Journal of Wind Engineering and Industrial Aerodynamics* 92, 1079–1130.
- Blocken, B., Carmeliet, J., Poesen, J., 2005. Numerical simulation of the wind-driven rain distribution over small-scale topography in space and time. *Journal of Hydrology* 315, 252–273.
- Blocken, B., Poesen, J., Carmeliet, J., 2006. Impact of wind on the spatial distribution of rain over micro-scale topography—numerical modelling and experimental verification. *Hydrological Processes* 20, 345–368.
- Choi, E.C.C., 1993. Simulation of wind-driven rain around a building. *Journal of Wind Engineering and Industrial Aerodynamics* 46 and 47, 721–729.
- Cornelis, W.M., Oltenfreiter, G., Gabriels, D., Hartmann, R., 2004a. Splash-saltation of sand due to wind-driven rain: vertical deposition flux and sediment transport rate. *Soil Science Society of America Journal* 68, 32–40.
- Cornelis, W.M., Oltenfreiter, G., Gabriels, D., Hartmann, R., 2004b. Splash-saltation of sand due to wind-driven rain: horizontal flux and sediment transport rate. *Soil Science Society of America Journal* 68, 41–46.
- Cornelis, W., Erpul, G., Gabriels, D., 2004c. The I.C.E. wind tunnel for wind and water interaction research. In: Visser, S., Cornelis, W. (Eds.), *Wind and Rain Interaction in Erosion*, Tropical Resource Management Papers, Chapter 13. Wageningen University and Research Centre, Wageningen, pp. 195–224.
- Cruse, R.M., Berghoefer, B.E., Mize, C.W., Ghaffarzadeh, M., 2000. Water drop impact angle and soybean protein amendment effects on soil detachment. *Soil Science Society of America Journal* 64, 1474–1478.
- De Lima, J.L.M.P., 1990. The effect of oblique rain on inclined surfaces: a nomograph for the rain-gauge correction factor. *Journal of Hydrology* 115, 407–412.
- De Lima, J.L.M.P., Van Dijk, P.M., Spaan, W.P., 1992. Splash-saltation transport under wind-driven rain. *Soil Technology* 5, 151–166.
- De Ploey, J., 1980. Some field measurements and experimental data on wind-blown sands. In: De Boodt, M., Gabriels, D. (Eds.), *Assessment of Erosion*. Wiley, Chichester, pp. 143–151.
- Ellison, W.D., 1947. Soil erosion studies. *Agricultural Engineer* 28, 145–146 (7 parts), 197–201; 245–248; 297–300; 349–351; 407–408; 447–450.
- Erpul, G., 1996. Determination of rainfall characteristics in a wind tunnel. M.Sc. Thesis, Ghent University, Ghent, 106 pp.
- Erpul, G., 2001. Detachment and sediment transport from interrill areas under wind-driven rains. Ph.D. Thesis. Purdue University, West Lafayette, IN.
- Erpul, G., Gabriels, D., Janssens, D., 1998. Assessing the drop size distribution of simulated rainfall in a wind tunnel. *Soil and Tillage Research* 45, 455–463.
- Erpul, G., Gabriels, D., Janssens, D., 2000. The effect of wind on size and energy of small simulated raindrops: a wind tunnel study. *International Agrophysics* 14, 1–7.
- Erpul, G., Norton, L.D., Gabriels, D., 2002. Raindrop-induced and wind-driven soil particle transport. *Catena* 47, 227–243.
- Erpul, G., Norton, L.D., Gabriels, D., 2003a. Sediment transport from interrill areas under wind-driven rain. *Journal of Hydrology* 276, 184–197.
- Erpul, G., Norton, L.D., Gabriels, D., 2003b. The effect of wind on raindrop impact and rainsplash detachment. *Transactions of the ASAE* 45, 51–62.
- Erpul, G., Norton, L.D., Gabriels, D., 2004. Splash-saltation trajectories of soil particles under wind-driven rain. *Geomorphology* 59, 31–42.
- Erpul, G., Gabriels, D., Norton, L.D., 2005. Sand detachment by wind-driven raindrops. *Earth Surface Processes and Landforms* 30, 241–250.
- Erpul, G., Gabriels, D., Cornelis, W.M., Samray, H.N., Guzelordu, T., 2008. Sand detachment under rains with varying angle of incidence. *Catena* 72, 413–422.
- Foulds, S.A., Warburton, J., 2007a. Wind erosion of blanket peat during a short period of surface desiccation (North Pennines, Northern England). *Earth Surface Processes and Landforms* 32, 481–488.
- Foulds, S.A., Warburton, J., 2007b. Significance of wind-driven rain (wind-splash) in the erosion of blanket peat. *Geomorphology* 83, 183–192.
- Furbish, D.J., Hamner, K.K., Schmeckle, M., Borosund, M.N., Mudd, S.M., 2007. Rainsplash of dry sand revealed by high-speed imaging and sticky paper splash targets. *Journal of Geophysical Research—Earth Surface* 112, (F1). doi:10.1029/2006JF000498.
- Gabriels, D., Cornelis, W., Pollet, I., Van Coillie, T., Quessar, M., 1997. The I. C. E. wind tunnel for wind and water erosion studies. *Soil Technology* 10, 1–8.
- Gilley, J.E., Finkner, S.C., 1985. Estimating soil detachment caused by raindrop impact. *Transactions of the ASAE* 28, 140–146.
- Gilley, J.E., Woolhiser, D.A., McWhorter, D.B., 1985. Interrill soil erosion. Part I: development of model equations. *Transactions of the ASAE* 28, 147–153, 159.
- Goossens, D., Poesen, J., Gross, J., Spaan, W., 2000. Splash drift on light sandy soils: a field experiment. *Agronomie* 20, 271–282.
- Grosh, J.L., Jarrett, A.R., 1994. Interrill erosion and runoff on very steep slopes. *Transaction of ASAE* 37, 1127–1133.
- Heymann, F.J., 1967. A survey of clues to the relation between erosion rate and impact parameters. *Second Rain Erosion Conference* 2, 683–760.
- Huang, C., Bradford, J.M., Cushman, J.H., 1982. A numerical study of raindrop impact phenomena: the rigid case. *Soil Science Society of America Journal* 46, 14–19.
- Huang, C., Bradford, J.M., Cushman, J.H., 1983. A numerical study of raindrop impact phenomena: the elastic deformation case. *Soil Science Society of America Journal* 47, 855–866.
- Jungerius, P.D., Verheggen, A.J.T., Wiggers, A.J., 1981. The development of blowouts in 'De Blink', a coastal dune area near Noordwijkerhout, The Netherlands. *Earth Surface Processes and Landforms* 6, 375–396.
- Jungerius, P.D., Dekker, L.W., 1990. Water erosion in the dunes. *Catena (Suppl.)* 18, 185–193.
- Kinnell, P.I.A., 1999. Discussion on 'The European Soil Erosion Model (EUROSEM): a dynamic approach for predicting sediment transport from fields and small catchments. *Earth Surface Processes and Landforms* 24, 563–565.
- Kinnell, P.I.A., 2005. Raindrop-impact-induced erosion processes and prediction: a review. *Hydrological Processes* 19, 2815–2844.
- Legout, C., Leguédou, S., Le Bissonnais, Y., Issa, O.M., 2005. Splash distance and size distributions for various soils. *Geoderma* 124, 279–292.
- Leguédou, S., Planchon, O., Legout, C., Le Bissonnais, Y., 2005. Splash projection distance for aggregated soils: theory and experiment. *Soil Science Society of America Journal* 69, 30–37.
- Moeyersons, J., 1983. Measurements of splash-saltation fluxes under oblique rain. *Catena (Suppl.)* 4, 19–31.
- Moeyersons, J., De Ploey, L., 1976. Quantitative data on splash erosion, simulated on unvegetated slopes. *Zeitschrift für Geomorphologie. Supplementband* 25, 120–131.
- Mouzai, L., Bouhadef, M., 2003. Water drop erosivity: effects on soil splash. *Journal of Hydraulic Research* 42, 61–68.
- Pedersen, H.S., Hasholt, B., 1995. Influence of wind speed on rainsplash erosion. *Catena* 24, 39–54.
- Poesen, J., 1985. An improved splash transport model. *Zeitschrift für Geomorphologie N.F.* 29, 193–221.
- Poesen, J., Savat, J., 1981. Detachment and transportation of loose sediments by raindrop splash. Part II: detachability and transportability measurements. *Catena* 8, 19–41.
- Quansah, C., 1981. The effect of soil type, slope, rain intensity and their interactions on splash detachment and transport. *Journal of Soil Science* 32, 215–224.
- Riezebos, H.T., Epema, G.F., 1985. Drop shape and erosivity. Part II. Splash detachment, transport and erosivity indices. *Earth Surface Processes and Landforms* 10, 69–74.
- Rutin, J., 1983. Erosional Processes on a Coastal Sand Dune, De Blink, Noordwijkerhout, Laboratory of Physical Geography and Soil Science, Univ. Amsterdam, The Netherlands.
- Savat, J., Poesen, J., 1981. Detachment and transportation of loose sediments by raindrop splash. Part I: the calculation of absolute data on detachability and transportability. *Catena* 8, 1–18.
- Sharma, P.P., Gupta, S.C., 1989. Sand detachment by single raindrops of varying kinetic energy and momentum. *Soil Science Society of America Journal* 53, 1005–1010.
- Sharon, D., 1970. Topography-conditioned variations in rainfall as related to the runoff contributing areas in a small watershed. *Israel Journal of Earth-Sciences* 19, 85–89.
- Sharon, D., 1980. The distribution of hydrologically effective rainfall incident on sloping ground. *Journal of Hydrology* 46, 165–188.
- Sharon, D., Arazi, A., 1997. The distribution of wind-driven rain in a small valley: an empirical basis for numerical model verification. *Journal of Hydrology* 201, 21–48.
- Sharon, D., Adar, E., Lieberman, G., 1983. Observations on the differential hydrological and/or erosional response of opposite-sloping slopes, as related to incident rainfall. *Israel Journal of Earth-Sciences* 32, 71–74.
- Sharon, D., Morin, J., Moshe, Y., 1988. Micro-topographical variations of rainfall incident on ridges of a cultivated field. *Transactions of the ASAE* 31, 1715–1722.
- Springer, G.S., 1976. *Erosion by Liquid Impact*. John Wiley and Sons, Inc., New York.
- Van Dijk, A.L.J.M., Meesters, A.G.C.A., Bruijnzeel, L.A., 2002. Exponential distribution theory and the interpretation of splash detachment and transport experiments. *Soil Science Society of America Journal* 66, 1466–1474.
- Van Heerden, W.M., 1964. *Splash erosion as affected by the angle of incidence of raindrop impact*. Unpublished Ph.D. thesis. Purdue University, Lafayette, Ind. USA.
- Vieira, G., Mora, C., Gouveia, M.M., 2004. Oblique rainfall and contemporary geomorphological dynamics (Serra da Estrela, Portugal). *Hydrological Processes* 18, 807–824.
- Visser, S.M., Sterk, G., 2007. Nutrient dynamics – wind and water erosion at the village scale in the Sahel. *Land Degradation and Development* 18, 578–588.
- Warburton, J., 2003. Wind-splash erosion of bare peat on UK upland moorlands. *Catena* 52, 191–207.
- Wright, A.C., 1986. A physically-based model of the dispersion of splash droplets ejected from a water drop impact. *Earth Surface Processes and Landforms* 11, 351–367.
- Wright, A.C., 1987. A method of the redistribution of disaggregated soil particles by rainsplash. *Earth Surf. Processes Landforms* 12, 583–596.